Rock and Soil Mechanics

Volume 44 | Issue 1 Article 4

3-13-2023

Analysis of longitudinal deformation of shield tunnel subjected to shield tail asymmetric thrust

Zhi-wei ZHANG
Faculty of Engineering, China University of Geosciences, Wuhan, Hubei 430074, China

Rong-zhu LIANG
Faculty of Engineering, China University of Geosciences, Wuhan, Hubei 430074, China, liangcug@163.com

Zhong-chao LI
Wuhan Municipal Construction Group Co., Ltd., Wuhan, Hubei 340023, China

Lian-wei SUN
Engineering General Institute, Shanghai Construction Group Co., Ltd., Shanghai 200080, China

See next page for additional authors

Custom Citation

ZHANG Zhi-wei, LIANG Rong-zhu, LI Zhong-chao, SUN Lian-wei, SHEN Wen, WU Wen-bing, . Analysis of longitudinal deformation of shield tunnel subjected to shield tail asymmetric thrust[J]. Rock and Soil Mechanics, 2023, 44(1): 88-98.

Analysis of longitudinal deformation of shield tunnel subjected to shield tail asymmetric thrust

Authors

Zhi-wei ZHANG, Rong-zhu LIANG, Zhong-chao LI, Lian-wei SUN, Wen SHEN, and Wen-bing WU

Rock and Soil Mechanics 2023 44(1): 88−98 ISSN 1000−7598
https: //doi.org/10.16285/j.rsm.2022.5191 rocksoilmech.researchcommons.org/journal

Analysis of longitudinal deformation of shield tunnel subjected to shield tail asymmetric thrust

ZHANG Zhi-wei[1], LIANG Rong-zhu[1], LI Zhong-chao[2], SUN Lian-wei[3], SHEN Wen[3], WU Wen-bing[1]

1. Faculty of Engineering, China University of Geosciences, Wuhan, Hubei 430074, China
2. Wuhan Municipal Construction Group Co., Ltd., Wuhan, Hubei 340023, China
3. Engineering General Institute, Shanghai Construction Group Co., Ltd., Shanghai 200080, China

Abstract: When the shield machine is driving along a curve alignment or during deviation correction, the asymmetrical thrust will generate an additional bending moment on the head of the segmental rings, which will cause longitudinal deformation of the shield tunnel. Current analytical methods commonly simplify the existing tunnel as an equivalent continuous beam, which will overlook the weakening of the circumferential joint. In this study, a simplified longitudinal beam-spring shield tunnel model (SLBSM) is established, which can simultaneously consider the opening and dislocation between segmental rings. Then, the shield tunnel under construction is simplified as an SLBSM resting on the Winkler foundation. The shield tunnel longitudinal deformation subjected to the shield tail asymmetric thrust is solved using the state space method; the reliability and applicability of the proposed method are verified by comparing with the results from finite element analysis and two existing continuous beam model. The parametric analysis is further performed to investigate the influences of some parameters on the deformation of shield tunnel. The results show that the longitudinal displacement of shield tunnel based on the continuous beam model exhibits continuous characteristics. While the longitudinal displacement predicted by the proposed method exhibits discontinuous characteristics, and “gaps” appear at the joints between adjacent segmental rings. Through the parametric analyses, it is found that increasing the rotation stiffness of the circumferential joint will effectively reduce the tunnel heave and opening of joint; increasing the shearing stiffness of the circumferential joint will effectively lead to the decrease of dislocation between adjacent segmental rings, but it will increase the tunnel heave and shear force; improving the foundation stiffness will effectively reduce the tunnel heave and opening of joint, but it will result in the increase of the dislocation between adjacent segmental rings. The effect of the axial force at the head of the segmental ring on the longitudinal deformation of the tunnel cannot be ignored. Increasing the axial force will effectively reduce the tunnel heave, opening of joint, and dislocation between adjacent segmental rings.

Keywords: asymmetric thrust; shield tunnel; longitudinal deformation; longitudinal beam-spring shield tunnel model; state space method

1 Introduction

With the rapid development of urbanization, urban subway transportation engineering is developing rapidly. Shield tunnelling method is widely used in the construction of subway tunnels due to its advantage of high efficiency, low cost, and minor impact on the surrounding environment[1−2]. However, curved tunneling and declination rectification will inevitably encountered while new shield tunnel is excavated in complex strata conditions and design requirements is very strict. Usually, the thrust of the oil cylinder jack in each partition at the tail of the shield machine is adjusted to carry out curved tunneling and deviation correction[3]. However, excessive asymmetrical jack thrust will in turn act on the segmental rings, causing cracks to the segment behind the shield tail, opening and dislocation between rings of tunnel, water leakage, and other hazards, which seriously threaten the overall safety of the tunnel[4−5]. Therefore, it is of great practical importance to reasonably evaluate the stress and deformation of the shield tunnel under asymmetric thrust.

The influence of eccentric jack thrust on the mechanical properties of shield tunneling is mainly reflected in the local stress concentration of segments and the longitudinal bending behavior of shield tunneling[6]. Many scholars around the world have conducted abundant research on the local mechanical properties of segment linings caused by asymmetric thrust and made a series of achievements mainly based on numerical methods. Song et al. [7] used the finite element method to study the stress deformation characteristics of the tunnel segments under the symmetric thrust of the shield tail during the construction period and found that the lining segment would produce local breakage between the 5th and 7th rings. Mo et al.[8] analyzed the deformation and stress of the tunnel

Received: 21 February 2022 Accepted: 22 May 2022
This work was supported by the National Natural Science Foundation of China (41807262), the Research Project of Wuhan Municipal Construction Group Co., Ltd. (wszky202013) and the Research Project of Shanghai Construction Engineering Group (19YF1421000).
First author: ZHANG Zhi-wei, male, born in 1999 Master degree candidate, focusing on urban pipe jacking tunnel protection. E-mail: zzw123ab@163.com
Corresponding: LIANG Rong-zhu, male, born in 1988, PhD, Associate Professor, Master's degree supervisor, research interests: structural safety of urban shield tunnels. E-mail: liangcug@163.com

lining under four types of extrusion with different attitude deflections, jacking forces, grouting pressure, and earth pressures, and found that the attitude change of the shield machine would cause large dislocation between the segments. Chaipanna et al.[9] analyzed the mechanical behavior of the lining under eccentric jack thrust during construction based on the nonlinear ground spring model combined with the finite element method. The results showed that the jack thrust had a significant effect on the axial and tangential directions of the tunnel lining. Nogales et al. [10] used the nonlinear three-dimensional finite element method to analyze the influence of the tunnel thrust on the segments and found that the eccentric thrust of the shield tail influenced the cracking performance of the segment.

However, limited studies have been conducted on the longitudinal deformation of shield tunnels due to asymmetric thrust. Talmon et al.[5] considered the tunnel under construction an Euler-Bernoulli beam model resting on a Winkler foundation and developed an analytical model of the lining response under asymmetric thrust during tunnel construction, but the Euler-Bernoulli (EB) beam did not reflect the shear deformation of the tunnel[11]. Wang et al.[4] further investigated the shear deformation of the tunnel. They treated the tunnel under construction as a Timoshenko (TM) beam model lying on the Winkler foundation and developed an analytical solution for the additional response of the shield tunnel under the asymmetric thrust.

In summary, the current analytical methods associated with longitudinal deformation of shield tunnels under asymmetric thrust are the same as those for the longitudinal deformation of existing shield tunnels under adjacent construction[12−15]. These studies treated shield tunnels as long continuous beams (i.e. EB and TM beams) on the elastic or inelastic foundation soil and used an equivalent method to estimate longitudinal stiffness of the tunnel. However, the continuous beam model ignores the difference in stiffness between the segmental rings and circumferential joints. In fact, due to the bolt connection between the rings of the shield tunnel, the stiffness of the joint is lower than that of the ring, resulting in the circumferential joints being the weak part of the shield tunnels.

Based on the limitations of the previous studies, the present study develops a simplified longitudinal beam-spring shield tunnel model (abbreviation SLBSM), which can consider the opening and dislocation between rings simultaneously. Then, the shield tunnel under construction is simplified as an SLBSM resting on the Winkler foundation. The longitudinal deformation of the shield tunnel subjected to the shield tail asymmetric jack thrust is solved using the state space method. Finally, the reliability and application of the proposed method are verified by comparing it with the results from the finite element method, TM continuous beam model, and EB continuous beam model. The sensibility analysis is further performed to investigate the influence of some parameters on the deformation of the shield tunnel.

2 Simplified longitudinal beam-spring shield tunnel model

Shield tunnel is a prefabricated lining structure, which consists of a series of segmental rings connected one by one by bolts to support the surrounding soil and prevent collapse into the tunnel. Since the bolt connection will make the stiffness of the joint lower than that of the rings, the circumferential joints are the weakest position of the shield tunnel, and the diseases of the shield segment, such as cracks, damage, dislocation, and water leakage, etc., all occur at the joints.

To fully reflect the structural characteristics of shield tunnel, a simplified longitudinal beam-spring shield tunnel model that can simultaneously consider the joint opening and shear dislocation between rings are proposed, as shown in Fig.1. The basic assumptions of this model are as follows:

(1) The shield tunnel consists of a series of short hollow beams connected by circumferential joints along the longitudinal direction

(2) The deformation of segmental rings of tunnel is simulated using EB short beams.

(3) Only rotation and dislocation deformation occur between segmental rings of tunnel, and the circumferential joints are simulated by rotation springs and shear springs.

(4) The variation of joint spring stiffness during tunnel deformation is not considered.

Based on the EB beam theory[16−17], the displacement, internal force, and geometric equations of the segmental rings can be obtained:

$$\varphi = -\frac{\mathrm{d}w}{\mathrm{d}y} \tag{1}$$

$$M = EI\frac{\mathrm{d}\varphi}{\mathrm{d}y},\ Q = \frac{\mathrm{d}M}{\mathrm{d}y} \tag{2}$$

$$\frac{\mathrm{d}Q}{\mathrm{d}y} = q(y) \tag{3}$$

where φ is the cross-section rotation of the tunnel; w is the longitudinal displacement of the tunnel; M, Q are the bending moment and shear force of the tunnel, respectively; EI is the bending rigidity of tunnel, E is the elasticity modulus, I is the moment of inertia; $q(y)$ is the external load acting on the tunnel; and y is the vertical coordinates.

As shown in Fig.1, the bending moment and shear force at the circumferential joints can be expressed by

$$M_j = k_\theta \cdot \Delta\varphi = k_\theta(\varphi_\mathrm{l} - \varphi_\mathrm{r}) \tag{4}$$

$$Q_j = k_s \cdot \Delta w = k_s (w_l - w_r) \quad (5)$$

where M_j, Q_j are the moment and shear force at the tunnel joint j; k_θ, k_s are the rotation stiffness and shear stiffness of the circumferential joints; $\Delta\varphi$, Δw denote the relative rotation angle and shear dislocation of the tunnel section at both sides of the joint; φ_r, φ_l are section rotation angles at right and left sides of tunnel joints; and w_r, w_l are section displacement at light and left sides of tunnel joints.

The established mode can more reasonably reflect the longitudinal deformation characteristics of the shield tunnel in practical engineering than the equivalent continuous beam model.

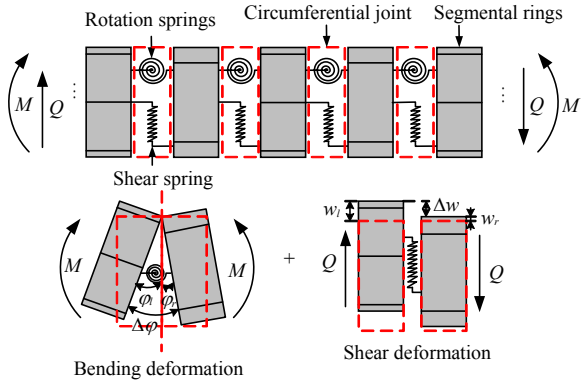

Fig. 1 Simplified longitudinal beam-spring shield tunnel model

3 Analytical model and theoretical derivation

3.1 Force analysis at the end of the tunnel

When the shield machine is driving along a curve or during derivation correction, the shield tail cylinder jack will act on the head of tunnel with asymmetric trust, and the additional moment generated by the asymmetric thrust at the head of tunnel is the essential reason[4]. Therefore, the grouting pressure and slurry hardening are not considered in this study. For convenience, the thrust of the oil cylinder in each partition of the shield tail is simplified as the concentrated load acting on the lining line of the segment, as shown in Fig.2. The asymmetrical thrust will lead to eccentric compression of the lining structure. We take the upper and lower the asymmetrical parallel force system as an example, and simplify them as the additional axial force P_o and additional moment M_e at the head of the tunnel. Thus, the expressions of P_o and M_e can be obtained as[18−19]

$$P_o = \sum_{i=1}^{m} P_i \quad (6)$$

$$M_e = \left[\left(\sum_{i=1}^{m/2} M_i^x \right)^2 + \left(\sum_{i=1}^{m/2} M_i^y \right)^2 \right]^{1/2} \quad (7)$$

$$M_i = R_s (P_i - P_{ip}) \quad (8)$$

where P_i denotes the thrust generated by the ith cylinder; m is the number of the cylinder; M_i is the moment generated by one pair of parallel forces P_i and P_{ip} at the shield tail; M_i^x and M_i^y are the components of the moment M_i on the x and y axes; and R_s is the distance from the jack cylinder to the axis of the shield machine.

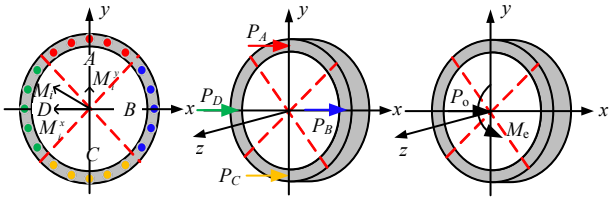

Fig. 2 Simplification of force system at tunnel head under asymmetric thrust

3.2 Shield tunnel longitudinal deformation

The shield tunnel under construction can be treated an SLBSM resting on a Winkler foundation model. Considering the one-way action of the segmental rings at the shield tail by the sealing brush and sealing grease, and the anchoring effect of the grout at the far end of the tunnel on the segmental rings, the head and end of the tunnel are regarded as simply supported and fixed constraints. The additional axial force P_o and additional bending moment M_e at the head of tunnel are shown in Fig. 3.

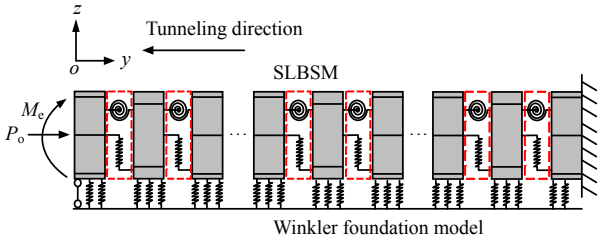

Fig. 3 Calculation model

According to simplification, Eqs. (2) and (3) can be further written as

$$M = EI \frac{\mathrm{d}\varphi}{\mathrm{d}y} + Nw = EI \frac{\mathrm{d}\varphi}{\mathrm{d}y} + P_o w \quad (9)$$

$$\frac{\mathrm{d}Q}{\mathrm{d}y} = kwD_t \quad (10)$$

where D_t is the tunnel diameter; k is the coefficient of ground reaction; which is a modified value proposed by Liang et al.[15] considering the arbitrary buried depth of the shield tunnel:

$$k = \frac{1.3E_s}{\omega D_t (1-\nu^2)} \sqrt[12]{\frac{E_s D_t^4}{EI}} \quad (11)$$

where E_s is the elastic modulus of ground; ω is tunnel buried depth influence coefficients, $\omega = 1 + 1/(1.7H_t/D_t)$; H_t is tunnel buried depth; and ν is the

Poisson's ratio of soil; Eq. (11) is only applicable for $H_t/D_t > 0.5$.

Transform Eqs. (1), (2), (9), and (10) into the following matrix form:

$$\frac{\mathrm{d}\boldsymbol{X}}{\mathrm{d}y} = \boldsymbol{A}\boldsymbol{X} \tag{12}$$

where $\boldsymbol{X}$ is the tunnel section state vector; and $\boldsymbol{A}$ is system matrix.

To ensure the calculation stability, Eq. (12) is further dimensionless, and the following state equation can be obtained:

$$\frac{\mathrm{d}\bar{\boldsymbol{X}}}{\mathrm{d}\bar{y}} = \bar{\boldsymbol{A}}\bar{\boldsymbol{X}} \tag{13}$$

where $\bar{\boldsymbol{X}}$ is the dimensionless state vector; $\bar{\boldsymbol{A}}$ is dimensionless system matrix.

$$\bar{\boldsymbol{X}} = \begin{bmatrix} \bar{w} & \varphi & \bar{Q} & \bar{M} \end{bmatrix} \tag{14}$$

$\bar{\boldsymbol{A}}$ is expressed as

$$\bar{\boldsymbol{A}} = \begin{bmatrix} 0 & -1 & 0 & 0 \\ -\bar{P}_o/\bar{I} & 0 & 0 & 1/\bar{I} \\ \bar{k}\bar{D}_t & 0 & 0 & 0 \\ 0 & 0 & 1 & 0 \end{bmatrix} \tag{15}$$

Dimensionless displacement and internal force can be written as

$$\left.\begin{aligned} &\bar{w} = \frac{w}{L}, \bar{y} = \frac{y}{L}, \bar{D}_t = \frac{D_t}{L}, \bar{Q} = \frac{Q}{EA}, \\ &\bar{M} = \frac{M}{EAL}, \bar{k} = \frac{kL^3}{EA}, \bar{I} = \frac{I}{AL^2}, \bar{P}_o = \frac{P_o}{EA} \end{aligned}\right\} \tag{16}$$

where L is the tunnel calculation length; and A is the tunnel section area.

According the matrix theory, the standard solution of Eq. (13) is

$$\bar{\boldsymbol{X}}(\bar{y}) = \bar{\boldsymbol{T}}(\bar{y} - \bar{y}_0)\bar{\boldsymbol{X}}_0 \tag{17}$$

where $\bar{\boldsymbol{X}}_0$ is the state vector at the head of the tunnel; $\bar{y}_0$ is the position of the head of the tunnel; $\bar{\boldsymbol{T}}$ is the transfer matrix, and can be written as

$$\bar{\boldsymbol{T}}(\bar{y} - \bar{y}_0) = \mathrm{e}^{\bar{\boldsymbol{A}}(\bar{y}-\bar{y}_0)} \tag{18}$$

Taking y=y_1, where y_1 is the end of a single tunnel ring, the matrix transfer relationship between the state vectors $\bar{\boldsymbol{X}}_0$ and $\bar{\boldsymbol{X}}_1$ at both sides of a single segmental ring of the tunnel can be obtained, i.e.,

$$\bar{\boldsymbol{X}}_1 = \bar{\boldsymbol{T}}(\bar{y}_1 - \bar{y}_0)\bar{\boldsymbol{X}}_0 \tag{19}$$

The existence of circumferential joints will lead to the weakening of the overall longitudinal stiffness of the tunnel. Figure 4 shows the deformation characteristics at the joints. According to the continuous conditions of shear and moment at the joints and combined with Eqs. (4) and (5), the expression of the internal force at the jth joint can be written as

$$M_0^{(j+1)} = M_1^{(j)} = M_j = k_\theta\left[\varphi_0^{(j+1)} - \varphi_1^{(j)}\right] \tag{20}$$

$$Q_0^{(j+1)} = Q_1^{(j)} = Q_j = k_s\left[w_0^{(j+1)} - w_1^{(j)}\right] \tag{21}$$

where $M_0^{(j+1)}$, $M_1^{(j)}$ are the bending moments at the right and left tunnel rings of the jth joint; $Q_0^{(j+1)}$, $Q_1^{(j)}$ are the shear forces at the right and left tunnel rings of the jth joint; $\varphi_0^{(j+1)}$, $\varphi_1^{(j)}$ are the rotation angles at the right and left tunnel ring side sections of the jth joint; $w_0^{(j+1)}$, $w_1^{(j)}$ are the displacements at the right and left tunnel rings of the jth joint.

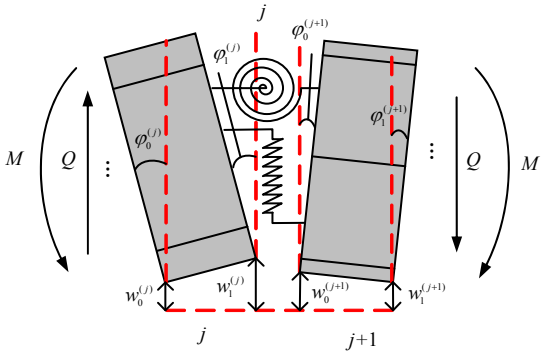

Fig. 4 Deformation of tunnel joint unit

Transform Eqs. (20) and (21) into following dimensionless matrix form:

$$\bar{\boldsymbol{X}}_0^{(j+1)} = \bar{\boldsymbol{J}}\bar{\boldsymbol{X}}_1^{(j)} \tag{22}$$

where $\bar{\boldsymbol{X}}_0^{(j+1)}$, $\bar{\boldsymbol{X}}_1^{(j)}$ are the state vectors of the right and left tunnel rings of the jth joint; and $\bar{\boldsymbol{J}}$ is the transfer matrix at the joint, and there is

$$\bar{\boldsymbol{J}} = \begin{bmatrix} 1 & 0 & 1/\bar{k}_s & 0 \\ 0 & 1 & 0 & 1/\bar{k}_\theta \\ 0 & 0 & 1 & 0 \\ 0 & 0 & 0 & 1 \end{bmatrix} \tag{23}$$

$\bar{k}_s$, $\bar{k}_\theta$ are the dimensionless rotation and shear stiffness of joints:

$$\bar{k}_s = \frac{k_s L}{EA}, \bar{k}_\theta = \frac{k_\theta}{EAL} \tag{24}$$

Equation (22) is the transfer relationship between the state vectors on the tunnel section at the left and right sides of the jth joint. For a shield tunnel containing n+1 segmental rings and n circumferential joints (see Fig.5), the transfer relationship between the state vector at the head and end of the overall tunnel can be obtained by combining Eqs. (19) and (22):

$$\bar{\boldsymbol{X}}_1^{(n+1)} = \bar{\boldsymbol{T}}^{(n+1)}\bar{\boldsymbol{X}}_0^{(n+1)} = \bar{\boldsymbol{T}}^{(n+1)}\bar{\boldsymbol{J}}\bar{\boldsymbol{X}}_1^{(n)} = \cdots = \bar{\boldsymbol{H}}\bar{\boldsymbol{X}}_0^{(1)} \tag{25}$$

where $\bar{\boldsymbol{H}}$ is the total transfer matrix, and there is

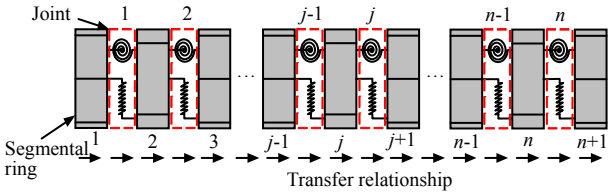

Fig. 5 Transmitting route of tunnel state vector

$$\bar{\boldsymbol{H}} = \bar{\boldsymbol{T}}^{(n+1)}\boldsymbol{J}\bar{\boldsymbol{T}}^{(n)} \cdots \bar{\boldsymbol{T}}^{(2)}\boldsymbol{J}\bar{\boldsymbol{T}}^{(1)} \tag{26}$$

Equation (25) contains eight unknown variables and can be solved with four boundary conditions. According to the calculation model, as shown in Fig.3, one end of the tunnel is fixed and the other end is simply supported, so the following boundary conditions can be obtained:

$$w_0^{(1)} = 0, M_0^{(1)} = M_e, w_1^{(n+1)} = 0, \varphi_1^{(n+1)} = 0 \tag{27}$$

Combining Eqs. (25) and (27), the state vector of the section at the head of the tunnel can be obtained,

$$\frac{\cos\psi + (\pi/2+\psi)\sin\psi}{\dfrac{\pi\cos^3\psi(1+nE_bA_bl_s/E_cA_cl_b)}{\psi\sin\psi+\cos\psi-\pi(0.5+nE_bA_bl_s/E_cA_cl_b)\sin\psi} - \left(\dfrac{\pi}{2}+\psi+\dfrac{1}{2}\sin 2\psi\right)} = \frac{P_o r}{2M_e} \tag{28}$$

$$\theta = \frac{l_s}{E_cI_c}\frac{\cos\psi + (\psi+\pi/2)\sin\psi}{\cos^3\psi}M \tag{29}$$

where E_c is the elastic modulus of the lining segment; I_c is the longitudinal inertial moment of the tunnel; n is the number of bolts at the joint; k_b is the average linear stiffness of bolts at joint, $k_b=E_bA_b/l_b$, E_b is the elastic modulus of the bolts, A_b is the section area of the bolt, l_b is the length of the bolts; l_s is the width of segmental rings; A_c is the section area of the segmental rings; and r is the position from the axis of the segment to the bolt.

According Eqs. (28) and (29), the rotation stiffness of circumferential joints k_θ can be obtained:

$$k_\theta = \eta\frac{E_cI_c}{l_s}\frac{\cos^3\psi}{\cos\psi+\left(\psi+\dfrac{\pi}{2}\right)\sin\psi} \tag{30}$$

where η is the rotation stiffness influence coefficients, and takes the value of 1 when joint reinforcement is not considered.

The joint opening Δ of tunnel can be obtained from the joint rotation angle as

$$\Delta = \tan\theta(r+r\sin\psi) \approx \frac{M_j}{k_\theta}(r+r\sin\psi) \tag{31}$$

The shear stiffness of circumferential joint is determined according to the equivalent shear stiffness calculation formula proposed by Wu et al. [11], i.e.,

$$k_s = \lambda\frac{1}{\dfrac{l_b}{n\kappa_bG_bA_b}+\dfrac{l_s-l_b}{\kappa_cG_cA_c}} \tag{32}$$

where κ_b and κ_c are the Timoshenko shear coefficient of the bolts and segmental rings, which are taken as 0.83 and 0.53; G_b and G_c are the shear stiffness of bolt and segmental ring, respectively, which are related to their elastic moduli, $G_b=E_b/[2(1+\nu_b)]$, $G_c=E_c/[2(1+\nu_c)]$; ν_b and ν_c are poisson's ratios of bolt and segmental ring, respectively; and λ is the influence coefficient of shear stiffness, its value is 1 without considering joint reinforcement.

and then the state vector at arbitrary section of the tunnel can be obtained according to Eqs. (17) and (22). Finally, the displacement and internal force at arbitrary section of the tunnel can be obtained according to Eq. (16).

3.3 Determination of rotational and shear stiffness of tunnel joint

The additional axial force P_o at the head of the tunnel will affect the rotation stiffness of the circumferential joints. According to the nonlinear equivalent bending stiffness theory considering the influence of longitudinal axial force established by Li et al. [20] and the calculation method of tunnel longitudinal equivalent bending stiffness proposed by Shiba et al. [21], the calculation formula for the rotation stiffness of circumferential joints considering longitudinal axial force is obtained. Regardless of the bolt pre-tightening force, there is the following relationship between the neutral axis angle ψ and the rotation angle θ:

4 Model comparison verification

To verify the applicability of the proposed method, the results obtained from the present solution are compared with those from the numerical simulation and the TM model method in the literature [4], and the EB model method. The longitudinal length (incorporating 50 rings) of the shield tunnel is analyzed. The width of each segmental ring l_s = 1.2 m, i.e. the length of the tunnel is L=60 m, and the buried depth of the tunnel is H_t =15 m; the structural parameters of the linings segments and joint bolts are shown in Tables 1 and 2; the elastic modulus of the foundation soil E_s=30 MPa, Poisson's ratio ν=0.3; according to Eqs. (30) and (32), the rotational stiffness k_θ and shear stiffness k_s of joints are 8.0×10^8 kN • m/rad and 2.2×10^6 kN/m; the additional moment M_e =11.4 MN • m and additional axial force P_o =8 MN at the head of the tunnel. Other detailed parameters can be found in the literature [4].

Table 1 Tunnel segmental rings parameters

Elastic modulus /MPa	Poisson's ratio	External diameter /m	Internal diameter /m	Thickness /m	Width /m
3.45×10^4	0.2	6.0	5.4	0.3	1.2

Table 2 Longitudinal joint bolts parameters

Elastic modulus /MPa	Poisson's ratio	Length /m	Diameter /m	Number of bolts
2.10×10^5	0.3	0.445	0.024	10

Figure 6(a) shows the comparison of the tunnel heave value calculated by the present solution with the TM model method in the literature [4], and the EB model method. It can be seen from Fig.6(a) that the heave value calculated by the present solution is slightly larger than the numerical value and the continuous beam results (i.e. TM model method and EB model method). Since the EB beam model cannot consider the shear deformation, the heave range of the tunnel is wider, and the position of the maximum heave of the tunnel is shifted towards the tail of the shield machine. It is further observed that the tunnel displacement curve calculated by the present solution is neither continuous nor smooth, consisting of a series of short straight lines with certain inclinations, and there are obvious jumps at the joints. However, the displacement curve calculated by the continuous beam model is smooth and continuous. This is because the established SLBSM considers the difference in stiffness between the segmental rings and joints of tunnel. The segmental rings are not prone to bend and shear deformation, and behave as a rigid body motion, while the joints are prone to rotation and dislocation deformation. In general, the method in this study and TM model method are consistent in the analysis of shield tunnel displacement under asymmetric thrust.

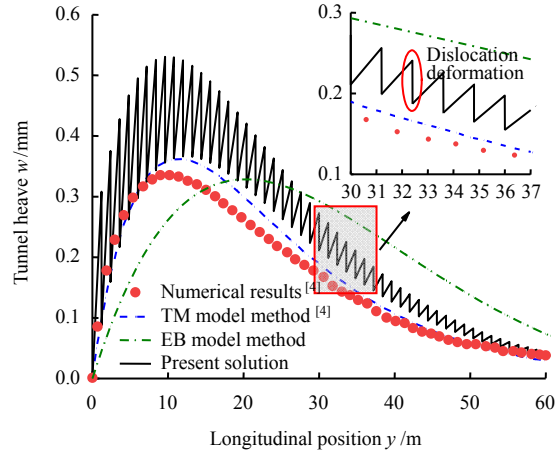

(a) Tunnel heave

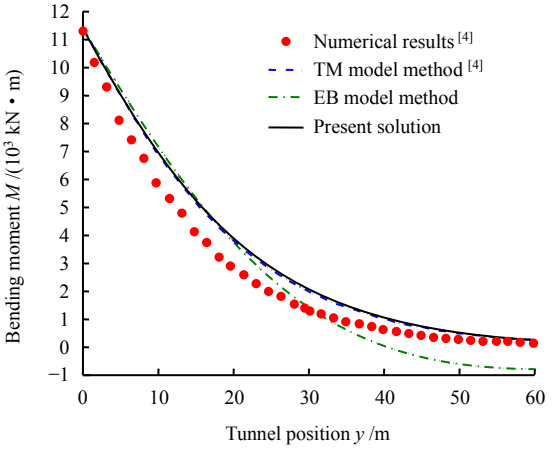

(b) Tunnel bending moment

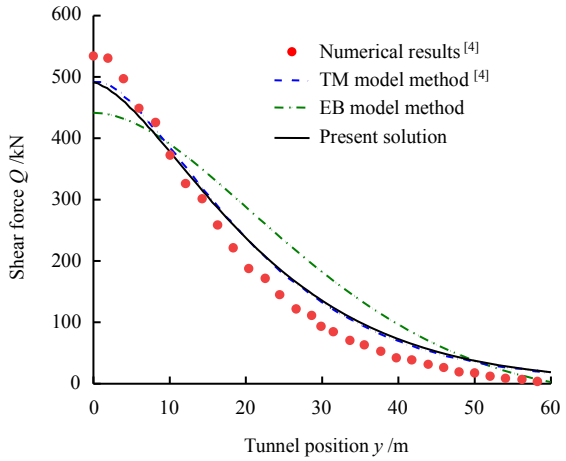

(c) Tunnel shear

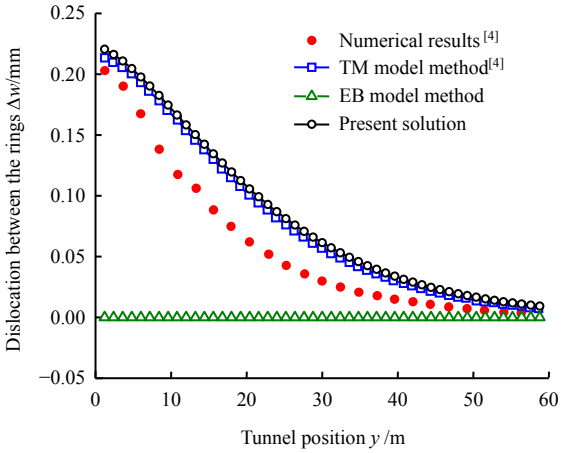

(d) Dislocation between the rings

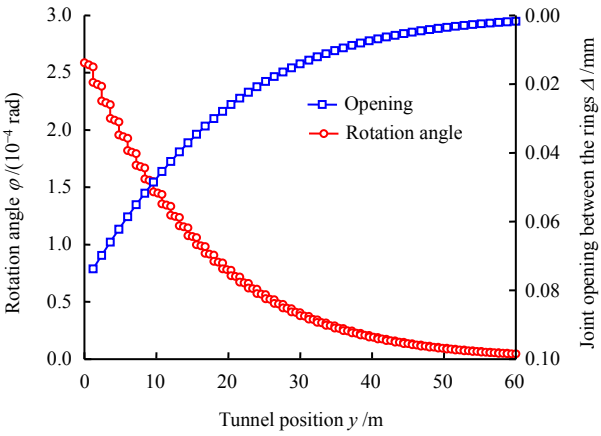

(e) Tunnel section rotation angle and joint opening between the rings

Fig. 6 Calculation of tunnel internal forces and deformation

Figure 6(b) gives a comparison of the bending moment of tunnel calculated by the present solution and numerical values and the TM model method in the literature [4], and the EB model method. It can be seen from the figure that the tunnel moment distribution obtained by the four methods is almost the same, the bending moment gradually decreases to zero along the longitudinal direction of the tunnel. In addition, the maximum bending moment occurs at the head of the tunnel, and its value is equal to the additional moment

M_e.

Figures 6(c) and 6(d) present the distribution of the shear force and dislocation between rings of tunnel calculated by the present solution, the EB model method, the numerical values and TM model method in the literature [4], respectively. It can be found that the distribution trends of the shear force and dislocation obtained by the present solution and TM model method are relatively consistent, and both gradually decrease to zero along the longitudinal direction of the tunnel, and are close to the numerical results.

The above results show that the maximum shear force occurs at the head of the tunnel, and the maximum displacement occurs between the first and second segmental rings, which is consistent with the position where the maximum bending moment and maximum opening occur, indicating that the maximum joint deformation of the shield tunnel subjected to asymmetric thrust occurs between the first and second segmental rings, so the shield tunnel should be given sufficient attention when shield machine is driving along a curve alignment or during deviation correction.

5 Parameter sensitivity analysis

In this section, the effects of joint rotation stiffness, joint shear stiffness, the ground elastic modulus, and the additional axial force at the head of tunnel on the longitudinal deformation of the shield tunnel under the asymmetric thrust are investigated. The number of tunnel rings used for calculation is 100, and the other calculation parameters are consistent with Section 4.

5.1 Effect of joint rotation stiffness

Figure 7 shows the variation of opening and dislocation between rings of tunnel under different joint rotation stiffness coefficients η. As can be seen from the figure, with the increase of η, joint opening gradually decreases to zero, while the dislocation between rings also gradually decreases, and the influence ranges of dislocation increases. When η increases from 10^{-2} to 10^{-1}, the opening and dislocation between the rings decrease sharply, with a maximum decrease of 5.5 mm and 0.38 mm. However, when η increases from 10^0 to 10^2, the tunnel ring opening and dislocation slightly decreases, the maximum reduction of ring opening is only 0.07 mm, and the maximum reduction of dislocation between the tunnel rings is only 0.09 mm.

Figure 8 shows the variation of the maximum tunnel heave under different joint rotation stiffness coefficients η. It can be found that the impact of joint rotation stiffness on the maximum tunnel heave is almost the same as that of joint rotation stiffness on the joint opening. When η is increased from 10^{-2} to 10^{-1}, the maximum tunnel heave decreases sharply by 4.4 mm. However, when the stiffness coefficient between the rings is further increased from 10^0 to 10^2, the maximum tunnel heave only decreases by 0.34 mm. This indicates that excessive reinforcement of the joint bending resistance has little contribution to reducing the heave and joint opening of tunnel. Therefore, in practical engineering, the circumferential joints can be appropriately strengthened, and excessive strengthening measures should not be adopted.

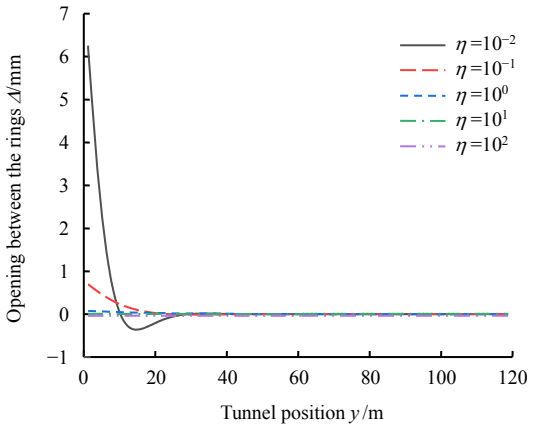

(a) Opening between the rings

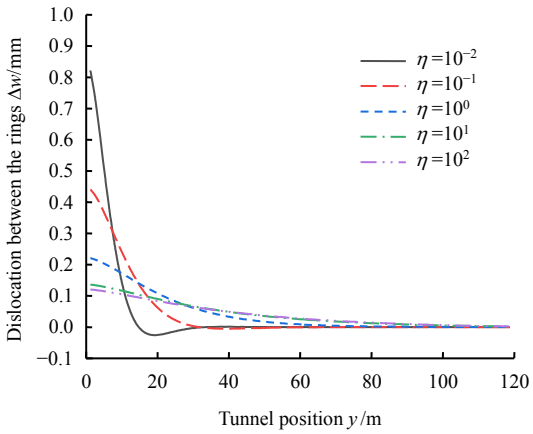

(b) Dislocation between the rings

Fig. 7 Effects of coefficient of rotation stiffness on the opening and dislocation between rings

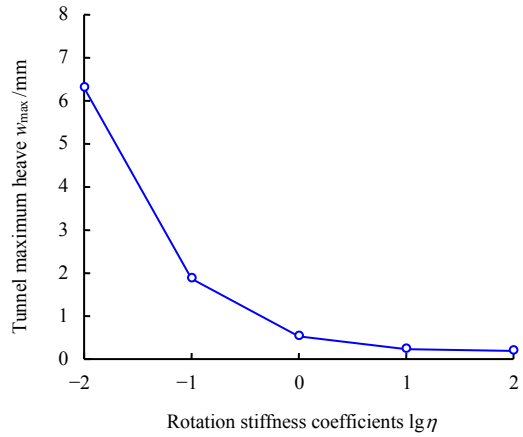

Fig. 8 Variation of the maximum tunnel heave under different joint rotation stiffness coefficients

5.2 Effect of joint shear stiffness

Figure 9 shows the variation of dislocation and opening between tunnel rings for different joint shear stiffness coefficients λ. It can be seen that with the increase of λ, the dislocation between rings gradually decreases to zero. However, the joint opening only affects the range, and its maximum value is not affected. When λ increases from 10^{-1} to 10^{0}, the dislocation between tunnel rings decreases sharply by 0.5 mm. But when λ increases from 10^{1} to 10^{3}, the dislocation between rings only decreases by 0.3 mm.

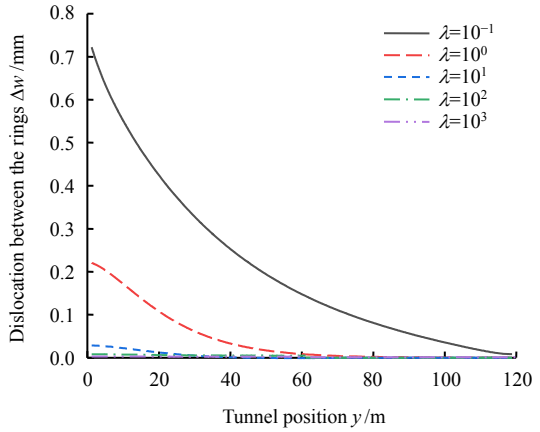

(a) Dislocation between the rings

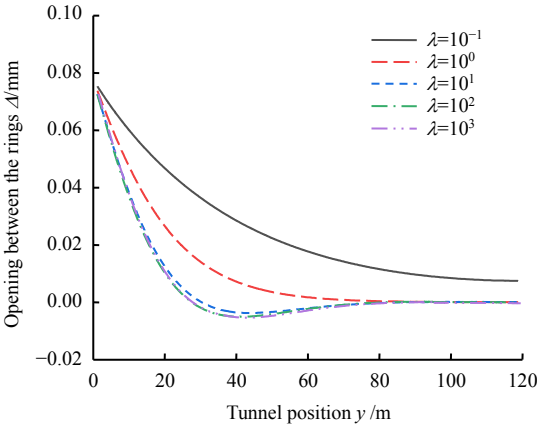

(b) Opening between the rings

Fig. 9 Effects of coefficient of shear stiffness on dislocation and opening between rings

Figure 10 shows the variation of maximum tunnel heave and shear force under different joint shear stiffness coefficients λ. As can be seen from the figure, with the increase of λ, the maximum shear shows a nonlinear increase, and the growth rate gradually slows down. However, it is noteworthy that different from the deformation law of existing shield tunnel due to adjacent construction, increasing the joint shear stiffness coefficient λ will increase the maximum heave of the tunnel, showing a nonlinear increase trend, and the rate gradually slows down. This is consistent with the conclusion in the literature [4] that increasing the equivalent shear stiffness of the tunnel will increase the maximum heave of the tunnel. The above results show that enhancing the shear stiffness of circumferential joints can reduce the dislocation between the rings, but it will lead to an increase in tunnel heave. Therefore, the joints should be properly reinforced in practical engineering.

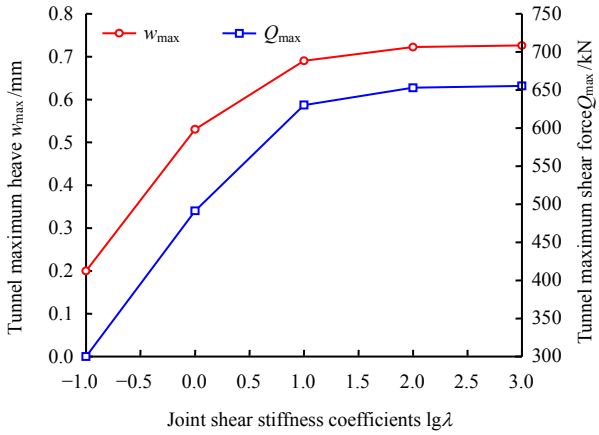

Fig. 10 Variations of the maximum tunnel heave and maximum shear forces under different joint rotation stiffness coefficients

In addition, compared with the equivalent continuous beam model, the proposed method can calculate the longitudinal deformation of the shield tunnel under the local reinforcement or failure at joints. The above calculation shows that the deformation between the segmental rings is dominated by dislocation, and the maximum dislocation deformation is located between the first and second rings. Therefore, to further evaluate the effect of local reinforcement or failure at joints on the longitudinal deformation of the tunnel under asymmetric thrust, the distribution of dislocation between the first and second rings when the shear stiffness of the first joint under three states is given in Fig.11. It can be seen that when the joint shear stiffness coefficient λ increases from 10^{-1} to 10^{1}, the dislocation between the first and second rings sharply decreases from 0.83 mm to 0.02 mm. However, the dislocations at the second to ninth joints increase slightly, while the other joints are almost unaffected. This indicates that the reinforcement of the joint between the first and second rings can effectively control the maximum dislocation deformation of the tunnel.

5.3 Effect of elastic modulus of foundation soil

Figure 12 shows the variation of the maximum opening and dislocation between tunnel rings under different ground elastic moduli E_s. Note that the maximum opening and dislocation between the rings are normalized. As can be seen from the figure, with the increase of E_s, the maximum opening and dislocation between the tunnel rings show opposite trends, the maximum opening gradually decreases with the increase

of E_s, while the maximum dislocation gradually increases with the increase of E_s. When $E_s \leqslant 50$ MPa, increasing E_s significantly increases the maximum dislocation and decreases the maximum opening between the tunnel rings. However, when $E_s > 50$ MPa, the elastic modulus of foundation soil has little effect on the opening and dislocation between rings of tunnel.

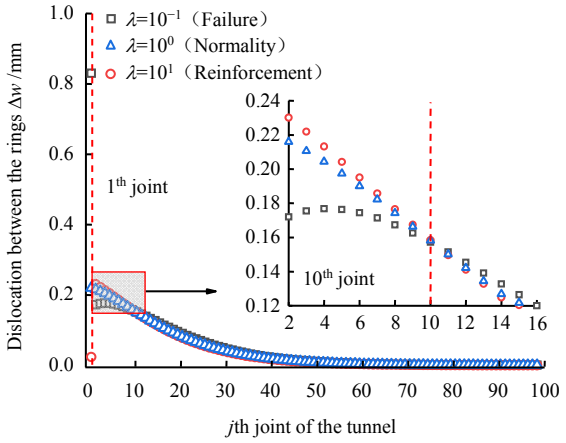

Fig. 11 Distribution of tunnel dislocation under three shear stiffness states of the first joint

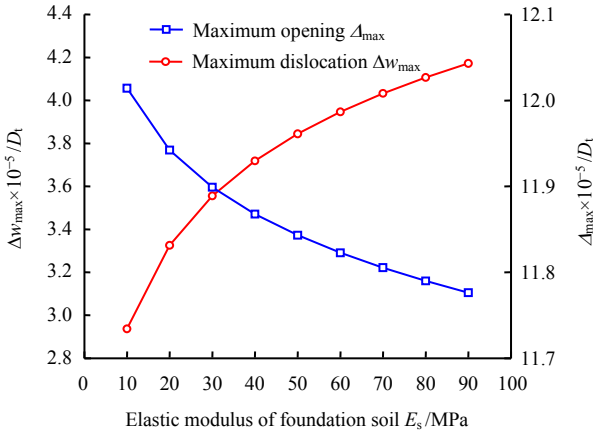

Fig. 12 Effects of the ground elastic modulus on maximum dislocation between adjacent segmental rings and the maximum opening of joint

Figure 13 shows the variation of tunnel heave with different ground elastic moduli E_s. The maximum heave is normalized by tunnel diameter. As can be seen from the figure, with the increase of E_s, the maximum tunnel heave exhibit a nonlinear decrease. When $E_s \leqslant 50$ MPa, the increase of E_s can significantly decrease the maximum heave, and when E_s increases from 50 MPa to 90 MPa, the increase of E_s has little contribution to maximum tunnel heave. The above results indicate that increasing the elastic modulus of the foundation soil can reduce the opening and heave, but it will lead to an increase in the dislocation between the rings. In addition, excessive reinforcement has little influence on the deformation of the tunnel.

5.4 Effect of additional axial force at the beginning of tunnel segments

The additional axial force at the head of tunnel will affect the bending resistance of the circumferential joints, thereby affecting the longitudinal deformation of the tunnel under the action of asymmetric thrust. Fig. 14 shows the variation of maximum opening and dislocation between segmental rings under different additional axial forces P_o. It can be seen that with the increase of P_o, the maximum opening and dislocation between the rings gradually decrease and trend to a constant, and both show the same change. When the axial force P_o increases from 0 MN to 6 MN, the opening and dislocation between the tunnel rings decrease sharply, with variations of 2.12 mm and 0.38 mm, respectively. As P_o continues to increase, the reductions of the maximum opening and dislocation between the rings gradually slow down and tend to 0 mm and 0.2 mm.

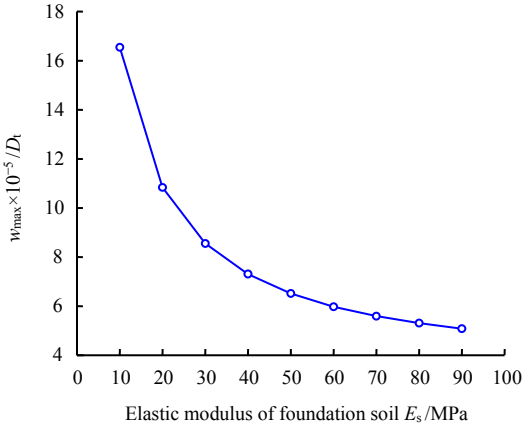

Fig. 13 Effects of ground elastic modulus on the maximum tunnel heave

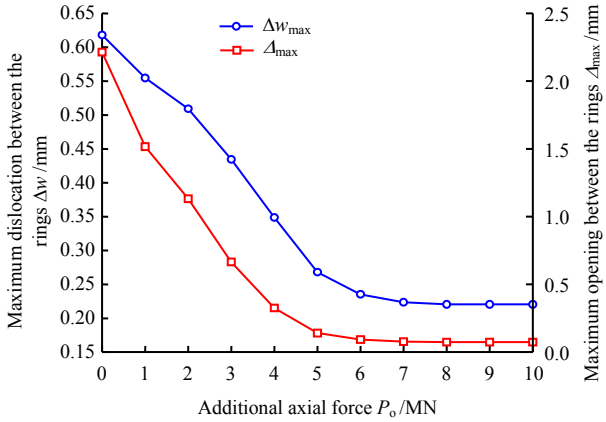

Fig. 14 Effects of additional axial force on the maximum dislocation between adjacent segmental rings and the maximum opening of joint

Figure 15 further shows the variation of tunnel heave under different additional axial forces P_o. When P_o <6 MN, increasing P_o can sharply decrease the maximum heave of the tunnel, however, continuing to increase P_o has little contribution to further reduce the

maximum heave of the tunnel. This indicates that increasing the axial force at the head of tunnel can significantly reduce the tunnel heave, the joint opening and the dislocation between rings. However, with the further increase of the axial force, it has little effect on the deformation of the tunnel.

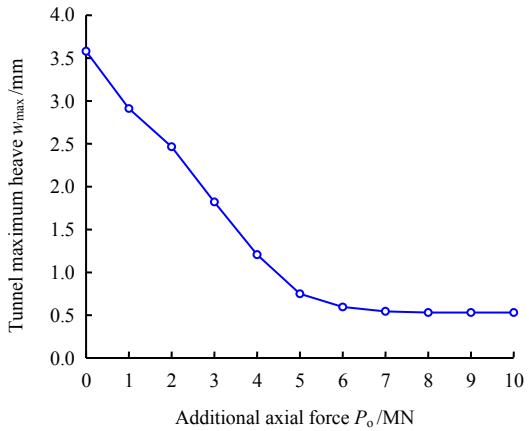

Fig. 15 Effects of the additional axial force on the maximum tunnel heave

6 Conclusion

(1) In this study, a simplified longitudinal beam-spring shield tunnel model is first established, which can simultaneously consider the opening and dislocation between segmental rings. Then, based on the SLBSM and Winkler foundation, the shield tunnel longitudinal deformation subjected to asymmetric jack thrusts is obtained using the state space method. The present solution is applicable to analyze the longitudinal deformation of the shield tunnel under the asymmetric jack thrusts without considering the variation of joint stiffness, or considering the reinforcement or failure of the local circumferential joints.

(2) The tunnel displacement obtained from the present solution is slightly larger than that from the Timoshenko beam model. Both the above two methods can reasonably predict the tunnel heave and joint deformations. However, a wider range of the tunnel displacement is obtained by the Euler-Bernoulli beam model, and the position of the maximum heave lean towards the shield tail that other methods. Moreover, the tunnel displacement curves calculated by the equivalent continuous beam models are continuous. However, the displacement curve of the tunnel obtained by the present solution is discontinuous, and the displacement will suddenly change at the joints.

(3) Increasing the rotation stiffness of circumferential joints can effectively reduce the opening between rings and heave of tunnel, but further increasing the rotation stiffness of joints will not contribute a lot to reducing the tunnel heave and opening between rings. In practical engineering, it is not appropriate to take excessive reinforcement measures for the joints.

(4) Increasing the shear stiffness of tunnel joints can effectively reduce the dislocation between segmental rings, but it will lead to an increase in heave and shear force of tunnel. In practical engineering, it is not advisable to strengthen only the joints at the largest dislocation position, and the joints within a certain range should be properly reinforced.

(5) Increasing the stiffness of the foundation soil can significantly reduce the gap between the tunnel rings and tunnel heave, but it will lead to an increase in the dislocation between the segmental rings, and excessive reinforcement does not further reduce tunnel deformation.

(6) The influence of the axial force at the head of tunnel on the tunnel deformation cannot be ignored. Increasing the axial force can significantly reduce the tunnel heave, joint opening and dislocation between rings. However, with the further increase of the axial force, its influence on the tunnel deformation is not significant.

References

[1] CHENG W C, NI J C, SHEN J S L, et al. Investigation into factors affecting jacking force: a case study[J]. Proceedings of the Institution of Civil Engineers-Geotechnical Engineering, 2017, 170(4): 322−334.

[2] LIU X X, SHEN S L, XU Y S, et al. Analytical approach for time-dependent groundwater inflow into shield tunnel face in confined aquifer[J]. International Journal for Numerical and Analytical Methods in Geomechanics, 2018, 42(4): 655−673.

[3] SHEN Xiang, YUAN Da-jun. Influence of shield pitch angle variation on shield-soil interaction[J]. Rock and Soil Mechanics, 2020, 41(4): 1366−1376.

[4] WANG Zu-xian, SHI Cheng-hua, LIU Jian-wen. Analytical solution of additional response of shield tunnel under asymmetric jack thrust[J]. Rock and Soil Mechanics, 2021, 42(9): 2449−2460.

[5] TALMON A M, BEZUIJEN A. Analytical model for the beam action of a tunnel lining during construction[J]. International Journal for Numerical and Analytical Methods in Geomechanics, 2013, 37(2): 181−200.

[6] HE Chuan, ZHANG Jing, FENG Kun. Research on structural analysis method of shield tunnels[J]. China Journal of Highway Transportation, 2017; 30(8): 1−14.

[7] SONG Ke-zhi, YUAN Da-jun, WANG Meng-shu. Segmental mechanical analysis of shield tunnel during construction stage[J]. Rock and Soil Mechanics, 2008, 29(3): 619−624.

[8] MO H H, CHEN J S. Study on inner force and dislocation of segments caused by shield machine attitude[J]. Tunnelling and Underground Space Technology, 2008, 23(3): 281−291.

[9] CHAIPANNA P, JONGPRADIST P. 3D response analysis of a shield tunnel segmental lining during construction and a parametric study using the ground-spring model[J]. Tunnelling and Underground Space Technology, 2019, 90: 369−382.

[10] NOGALES A, DE LA FUENTE A. Crack width design approach for fibre reinforced concrete tunnel segments for TBM thrust loads[J]. Tunnelling and Underground Space Technology, 2020, 98: 103342.

[11] WU H N, SHEN S L, LIAO S M, et al. Longitudinal structural modelling of shield tunnels considering shearing dislocation between segmental rings[J]. Tunnelling and Underground Space Technology, 2015, 50: 317−323.

[12] KANG Cheng, YE Chao, LIANG Rong-zhu, et al. Nonlinear longitudinal deformation of underlying shield tunnel induced by excavation[J]. Chinese Journal of Rock Mechanics and Engineering, 2020, 39(11): 2341−2350.

[13] LIANG Rong-zhu, LIN Cun-gang, XIA Tang-dai, et al. Analysis on the longitudinal deformation of tunnels due to pit excavation considering the tunnel shearing effect[J]. Chinese Journal of Rock Mechanics and Engineering, 2017, 36(1): 223−233.

[14] LIANG R. Simplified analytical method for evaluating the effects of overcrossing tunnelling on existing shield tunnels using the nonlinear Pasternak foundation model[J]. Soils and Foundations, 2019, 59(6): 1711−1727.

[15] LIANG R, WU W, YU F, et al. Simplified method for evaluating shield tunnel deformation due to adjacent excavation[J]. Tunnelling and Underground Space Technology, 2018, 71: 94−105.

[16] HUANG H W, GONG W P, KHOSHNEVISAN S, et al. Simplified procedure for finite element analysis of the longitudinal performance of shield tunnels considering spatial soil variability in longitudinal direction[J]. Computers and Geotechnics, 2015, 64: 132−145.

[17] LIANG R, XIA T, HONG Y, et al. Effects of above-crossing tunnelling on the existing shield tunnels[J]. Tunnelling and Underground Space Technology, 2016, 58: 159−176.

[18] SHI C H, WANG Z X, GONG C J, et al. Prediction of the additional structural response of segmental tunnel linings induced by asymmetric jack thrusts[J]. Tunnelling and Underground Space Technology, 2022, 124: 104471.

[19] LIANG Rong-zhu, XIA Tang-dai, LIN Cun-gang, et al. Control of the shield's vertical attitude during shield tunnelling in soft soils[J]. Modern Tunnelling Technology, 2015, 52(5): 152−157.

[20] LI P, DU S J, SHEN S L, et al. Timoshenko beam solution for the response of existing tunnels because of tunneling underneath[J]. International Journal for Numerical and Analytical Methods in Geomechanics, 2016, 40(5): 766−784.

[21] SHIBA Y, KAWASHIMA K, OHIKATA M, et al. Calculation method on sectional forces of longitudinal structure of shield tunnel under earthquake force based on response deformation method[J]. Journal of Japan Society of Civil Engineers, 1989, 404: 385−394.